ISEC 2024 – 3rd International Sustainable Energy Conference
Heat Pumping Technologies and System Integration
https://doi.org/10.52825/isec.v1i.1158

Published: 24 Apr. 2024

Energetic Potential of Parallel Operation of Two Heat Sources in a Dual-Source Heat Pump

Tobias Reum[1,*], David Schmitt[1], Thorsten Summ[1], and Tobias Schrag[1]

[1] Technische Hochschule Ingolstadt, Germany

*Correspondence: Tobias Reum, tobias.reum@thi.de

Abstract. Dual-source heat pumps can mitigate disadvantages of single source heat pumps: They have fewer geological requirements compared to ground-source heat pumps while having higher efficiencies compared to air-source heat pumps. Parallel operation of two heat sources can also make electric heaters for peak loads obsolete, leading to economic benefits in the operational costs. Parallel operation has not been analysed thoroughly at different evaporation temperature gradients. To address this gap in research, four possible interconnections of two heat sources were analysed using a refrigerant cycle simulation, two with similar and two with separate evaporation pressures. The energetic potential of each interconnection is evaluated and compared to single source operation with an air-source and a ground-source heat pump. The results showed that only the interconnections with separate evaporation pressure allowed significant reduction in evaporation power from the ground source. As expected, the efficiency – compared to single air-source operation – increased for all parallel interconnections but decreased compared to ground-source operation. Efficient peak load coverage with small ground-source collectors therefore requires a more complex interconnection of completely split evaporator branches at different evaporation pressures. While the efficiency and heating power compared to single ground-source operation decreased slightly (by 4% and 6%, respectively), the power load on the GSHX and ASHX reduced to about 54% and 66% compared to the corresponding single-source operation, respectively. This allows high efficiency at reduced GSHX size and ASHX noise emission. Additionally, this interconnection also allows increased flexibility for improved heat source management.

Keywords: Dual-Source Heat Pump, Parallel Operation, Refrigerant Cycle Simulation, Peak Load, Noise Reduction, Simscape Modelling

1. Introduction

Dual-source heat pumps (DSHPs) are a growing focus in current research. A common combination is a ground-source heat exchanger (GSHX) with an air-source heat exchanger (ASHX). [1]. These systems can minimize the disadvantages of ground-source heat pumps (GSHP), which usually are geological requirements and allowances for borehole heat exchangers and space requirements for shallow ground source heat exchangers, and air-source heat pumps (ASHP), usually low efficiency during winter and noise emissions. These disadvantages limit GSHP and ASHP usability especially in more densely populated regions, e.g. urban areas [2].

GSHX technologies range from boreholes over shallow horizontally distributed heat exchangers to specifically shaped collectors, usually for shallow, but vertical installation (e.g. basket types). The first usually requires extensive allowances and geological requirements. The latter technologies have large space requirements, making installation possible only in larger gardens. With DSHPs, several researches report a reduction in GSHX size of up to 50% while

maintaining comparable annual efficiencies to conventional GSHPs [3–5], allowing either installation of smaller GSHX sizes or retrofitting of undersized GSHX. Most of this research has focussed on the energy reduction from the GSHX by serial utilization of either the GSHX or a different heat source (like ASHX or solar thermal collectors).

Similarly, most heat pump capacities are designed to not cover the full peak heating load of the building. Especially ASHPs' heating power drops significantly in cold ambient air conditions, requiring further measures. Thermal building mass, buffer storages and electric heaters are used to cover these peak heating loads. Especially electric heaters, however, lead to efficiency reductions. This leads to low overall heat pump efficiencies during heating-dominant winter months. Parallel operation of two (smaller, according to the previous section) heat sources can reduce the need for oversizing and / or electric heaters.

DSHPs can also reduce the noise emissions by reducing the power extracted from the ASHX. One major noise emission source is the ventilator of the outdoor evaporation unit. A reduction in ASHX evaporation power allows a reduction of the ventilator power and thus the noise emissions. Again, parallel operation of a DSHP can limit the power required from an ASHX and enables this adaptation of the ventilator speed.

Several researchers have investigated options to include parallel operation of two heat sources within a single heat pump to efficiently cover the peak load while reducing the load on the GSHX. Some propositions combined several heat sources on a similar evaporation pressure (e.g. [6, 7]). On similar temperature levels, this allows increased efficiencies and less heat extraction from either heat source. However, detailed analyses are missing on the potential when there is a notable temperature gradient between the heat sources. Qiu et al. [8] and Bertsch et al. [9] have analysed several combinations of air-source heat pumps and a secondary heat source consisting of solar thermal collectors. Here, the solar thermal heat source was always on a higher temperature level, limiting the interconnection requirements by having a strict temperature gradient between the heat sources. Another research developed fully flexible interconnection using air- and ground-source heat exchangers [10]. Here, fully separated evaporator branches (including expansion valve and compressor) allowed parallel operation of both heat sources feeding into the same condenser for heating purposes. However, energetic benefits were only measured experimentally at a limited number of boundary conditions and not compared to other interconnections with comparable refrigerant cycle design.

1.1 Research question

There has been no comparative analysis of the different approaches for parallel operation under similar boundary conditions in research. This work aims to fill this research gap with several interconnections from literature combining an ASHX with a GSHX. The aim is to allow the decision, which interconnection is to be used for which of the following objectives: (a) to increase the efficiency at peak loads, i.e. low ambient temperatures; (b) to reduce the power load on the GSHX at various temperature gradients between the heat sources to increase flexibility of heat source design and management; and (c) to reduce the load on the ASHX at various temperature gradients between the heat sources to allow ventilator power reduction during noise-vulnerable time periods throughout the day (e.g. during the night).

2. Methodology

First, benchmarks are simulated using single source heat pumps, both GSHP and ASHP. Next, four interconnections for parallel operation are selected from literature and their schematics shown in Figure 1:

(1) is an interconnection based on a patent by Behrmann [6]. One evaporator is located in series after the other on similar pressure levels, i.e. no valve in between. In this case, the air evaporator is located after the brine evaporator.
(2) is an interconnection based on the so-called “low-temperature heat-collecting system” by Qiu et al. [8]. This interconnection can be used with ASHX and GSHX (instead of a solar thermal heat source used in their work) due to the proposed usage of the secondary heat source working at close to the other evaporation pressure. This is achieved by controlling the refrigerant flow through each evaporator with an expansion valve, but only using one single compressor stage. The economizer, proposed in their research, is neglected for comparability reasons.
(3) is based on interconnection (1) but introduces a medium pressure level using an expansion valve between the evaporators. The in-between expansion valve is controlled to a vapor quality of 60% between the evaporators, thus having a similar evaporation power ratio between the heat sources.
(4) is an interconnection based on a proposal by Reum et al. [10], having both evaporators in parallel with separate evaporation pressures. This is achieved by two expansion valves and compressors in each evaporator branch. In this research, the mass flow of each compressor is halved to allow comparable total refrigerant mass flows with the other interconnections.

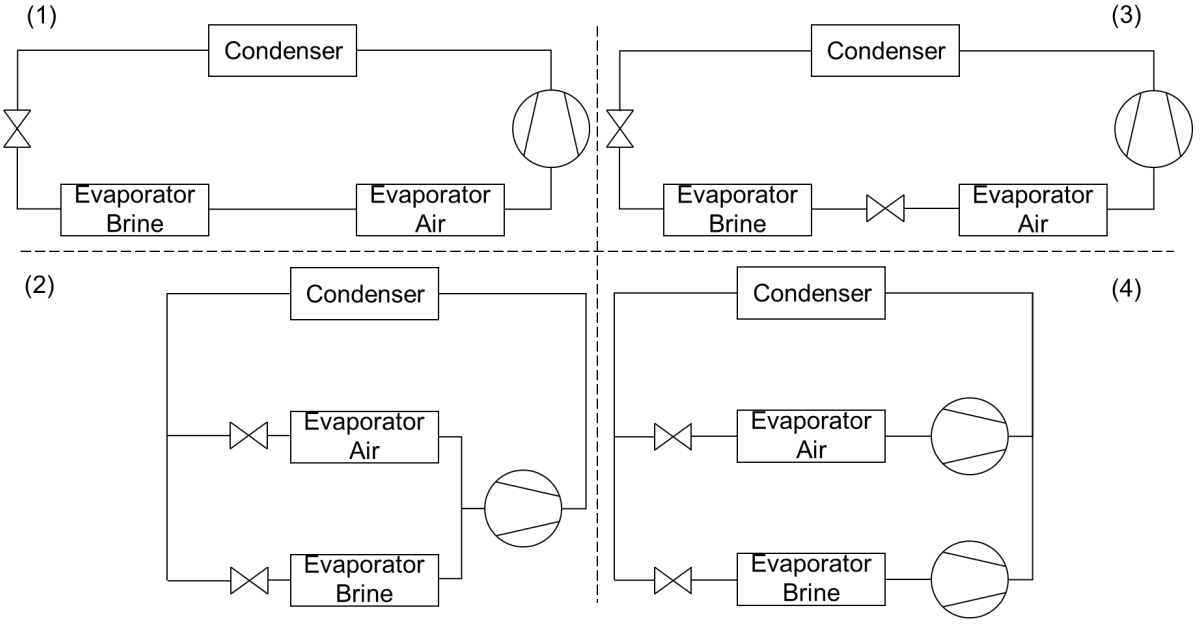

***Figure 1**: The four analyzed refrigerant cycle interconnections. (1) evaporation on similar pressure level in series; (2) evaporation on similar pressure level in parallel; (3) evaporation on different pressure levels in series; (4) evaporation on different pressure levels in parallel.*

The brine inlet temperature of the GSHX is set to 5 °C. To account for the varying temperature gradients between the sources, the inlet ambient air conditions are set to −5, 5, 15 °C respectively. The sink inlet temperature of the water is set to 30 °C. The mass flows of the brine, air and water flows (1, 5 and 1 kg/s, respectively) were kept constant over all simulations. This allows momentary efficiency and power evaluation of all four interconnections including the single source benchmarks. Table 1 shows the temperature parameters for the simulations.

***Table 1**: Boundary conditions for the refrigerant cycle simulations.*

Interconnection	T_{brine} in °C	T_{air} in °C	$T_{heating}$ in °C
Air-source	-	−5	30
	-	5	30

	-	15	30
Ground-source	5	-	30
(1),(2),(3),(4)	5	−5	30
	5	5	30
	5	15	30

The refrigerant cycles are designed and simulated using the physical modelling and simulation language MATLAB/Simscape for the comparison. Simscape models each component one-dimensionally with a differential equation for the dynamics and a mass and energy continuity equations. The results were taken at steady state.

Two-phase fluid components are used for the refrigerant cycle. Thermal liquid is applied to the brine source of the GSHX and the heat sink cycle at the condenser. Moist air serves as the source medium for the ASHX. System-level heat exchangers are used for the heat sources and the heat sink, each designed for single family houses (about 7 kW each). Compressor and source and sink pumps / ventilators are modelled with controlled mass flow sources. The isentropic compressor uses a mass flow according to real data sheets [11] (capacity of around 7.5 kW in the simulated boundary condition range). Sinks and sources are supplied by infinitely large reservoirs at set temperatures. This allows similar heat exchanger sizes, temperature levels and mass flows. The electronic expansion valve controlling the superheat before compressor inlet to 4 °C is a variable opening orifice with a PID controller for the control member position. A refrigerant accumulator is added to buffer refrigerant and guarantee liquid refrigerant flow to the expansion valve. As the refrigerant medium, R454B was used [12].

2.1 Comparison parameters

The main comparison parameters were the Coefficient of Performance (COP), the heating power, the power extracted from the GSHX and from the ASHX. The COP was calculated by:

$$\mathrm{COP} = \frac{\dot{Q}_{\mathrm{heat}}}{P_{\mathrm{el}}}, \tag{1}$$

with the heating power $\dot{Q}_{\mathrm{heat}}$ and the electrical power P_{el}. The heating power was derived from the change in enthalpy of the refrigerant over the condenser using the specific enthalpy h at the condenser inlet and outlet and the mass flow of the refrigerant across the condenser $\dot{m}_{\mathrm{cond}}$:

$$\dot{Q}_{\mathrm{heat}} = \dot{m}_{\mathrm{cond}} * (h_{\mathrm{cond,out}} - h_{\mathrm{cond,in}}). \tag{2}$$

The electrical power is the mechanical power of the compressor with added electrical inefficiencies. In this simulation, a perfect electric motor as well as an isentropic compressor was assumed. Therefore, the electric compressor power can be similarly calculated using:

$$P_{\mathrm{el}} = \dot{m}_{\mathrm{comp}} * (h_{\mathrm{comp,out}} - h_{\mathrm{comp,in}}). \tag{3}$$

The thermal power extracted from the GSHX $\dot{Q}_{\mathrm{evap,GSHX}}$ and the ASHX $\dot{Q}_{\mathrm{evap,ASHX}}$ are calculated using the same method:

$$\dot{Q}_{\mathrm{evap,GSHX}} = \dot{m}_{\mathrm{evap,GSHX}} * (h_{\mathrm{evap,GSHX,out}} - h_{\mathrm{evap,GSHX,in}}), \tag{4}$$

$$\dot{Q}_{\mathrm{evap,ASHX}} = \dot{m}_{\mathrm{evap,ASHX}} * \left(h_{\mathrm{evap,ASHX,out}} - h_{\mathrm{evap,ASHX,in}}\right). \quad (5)$$

3. Results

The simulations conducted reveal the following results as shown in Table 2. Depicted are the comparison parameters according to section 2.1. Due to the isentropic compression, the COPs are high compared to real heat pumps. The comparability with each other, however, is still reasonable and the focus of this research. The results are being discussed more in detail in the following paragraphs.

***Table 2**: Resulting comparison parameters of the refrigerant cycle simulation.*

Interconnection	T_{air} in °C	COP in -	$\dot{Q}_{\mathrm{heat}}$ in kW	P_{el} in kW	$\dot{Q}_{\mathrm{evap,GSHX}}$ in kW	$\dot{Q}_{\mathrm{evap,ASHX}}$ in kW
Air-source (single mode)	−5	4.72	3.17	0.67	-	2.50
	5	6.82	4.94	0.72	-	4.21
	15	8.57	6.45	0.75	-	5.70
Ground-source (single mode)	5	6.83	4.94	0.72	4.22	-
(1)	−5	5.89	4.12	0.70	3.37	0.05
	5	7.32	5.38	0.74	2.55	2.10
	15	8.23	6.16	0.75	0.53	4.89
(2)	−5	5.66	3.91	0.69	2.95	0.27
	5	6.02	4.23	0.70	1.82	1.71
	15	6.88	4.99	0.73	0.45	3.81
(3)	−5	5.34	3.69	0.69	1.54	1.47
	5	6.41	4.69	0.73	1.97	1.99
	15	7.18	5.65	0.79	2.29	2.58
(4)	−5	6.52	4.65	0.71	2.29	1.65
	5	7.21	5.29	0.73	2.28	2.27
	15	8.29	6.16	0.74	2.27	3.16

As a plausibility check, the pressure-enthalpy diagram is used for comparison and to draw first conclusions about the operation of each interconnection. Figure 2 shows the pressure-enthalpy diagrams for the simulations with T_{air} = −5 °C. The following paragraphs go more into detail on the behavior at this ambient temperature. The condensation pressure (between points 4 and 1) varies slightly due to the different heating powers being transferred to the water cycle using the same heat exchanger. The evaporation pressures (between points 2 and 3) vary with the source temperatures and the interconnection. This results in different compressor powers which translate to the (idealized) electrical power.

First, the benchmarks show results as expected. The evaporation pressure for the air-source operation is significantly lower than for the ground-source operation at 5 °C brine temperature (constant across all simulations). The superheat is properly controlled to the set 4 °C, seen by the evaporation lasting into the gaseous zone to the right. As a result, the heating power as well as the COP is significantly higher for the ground-source.

Interconnection (1) shows a higher heating power and COP than air-source (see Table 2), but lower values than ground-source. The pressure-enthalpy diagram shows barely any power on the ASHX evaporator, while the evaporation pressure is close to the air-source evaporation pressure. The reduction of ground-source evaporation power is low compared to the single ground-source operation (about 20%, as seen in Table 2). This indicates a low benefit to peak

load reduction on the GSHX using single ground-source operation at this temperature gradient between the heat sources.

Interconnection (2) shows a similar behavior as interconnection (1). While not as clear in the pressure-enthalpy diagram (due to specific enthalpy values shown in the diagram neglecting the different mass flows through each evaporator), Table 2 shows the differences more clearly: The load on the GSHX is slightly reduced, the ASHX barely supports the parallel operation with less about 0.27 kW (or less than 10% of the total evaporation power).

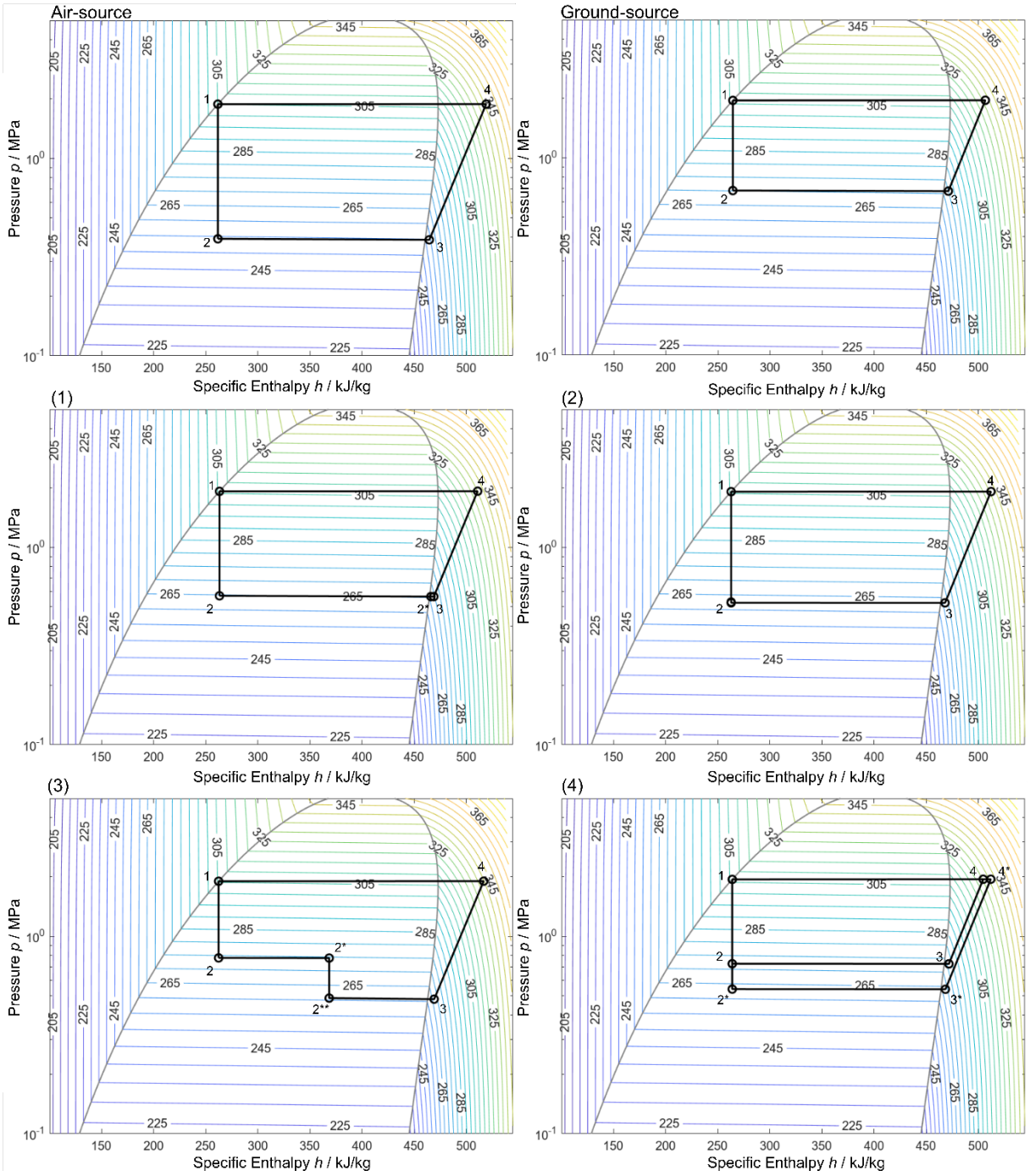

***Figure 2**: Pressure-enthalpy diagrams for the stable operation points of the refrigerant cycle simulations. The boundary condition for the ambient air is −5 °C. Indicated are the states at four numbered refrigerant sections: 1 high pressure liquid; 2 low pressure gas-liquid; 3 low pressure superheated gas; 4 high pressure hot gas. Stars indicate separate evaporation pressure levels or part-evaporation. 1 → 2 is the isenthalpic expansion; 2 → 3 is the isobaric evaporation including overheating; 3 → 4 is the isentropic compression; 4 → 1 is the isobaric condensation including gas cooling.*

Interconnection (3) shows an almost even distribution of the evaporation powers. The pressure drop after part-evaporation in the GSHX is significant. This leads to an overall efficiency increase compared to air-source operation (see Table 2). However, this interconnection leads to high superheat at compressor inlet, in turn leading to increased hot gas temperatures at compressor outlet. This is more predominant at higher ambient air temperatures and might lead to shorter service time.

Interconnection (4) shows the separate, parallel evaporation process. This allows optimal evaporation at both heat sources. The evaporation powers are split accordingly and result in overheating temperatures of 4 °C at both compressor inlets.

3.1 Energetic performance comparison

The energetic performance of the interconnections is shown mainly by the parameters efficiency (COP) and heating power. Figure 3 shows the COP of the benchmarks as well as the four interconnections versus the ambient temperature. Since the GSHP operation has a constant brine inlet temperature, the COP is stable in relation to the ambient temperature. The air shows a positive gradient towards higher COP at higher ambient temperatures. Interconnections (2) and (3) only show a higher COP at low ambient temperatures compared to single ASHP operation. At similar evaporation temperatures, the COP is lower than either single-source operation and at higher ambient temperatures, the COP is barely higher than GSHP operation. The other two interconnections (1) and (4) show only a slight decrease of the COP at high ambient temperatures compared to ASHP and a higher COP than single-source operation at comparable evaporation temperatures. However, at low ambient temperatures, only interconnection (4) shows a COP barely lower than pure GSHP operation. As described in section 3., this is mainly due to the optimal evaporation at both heat sources.

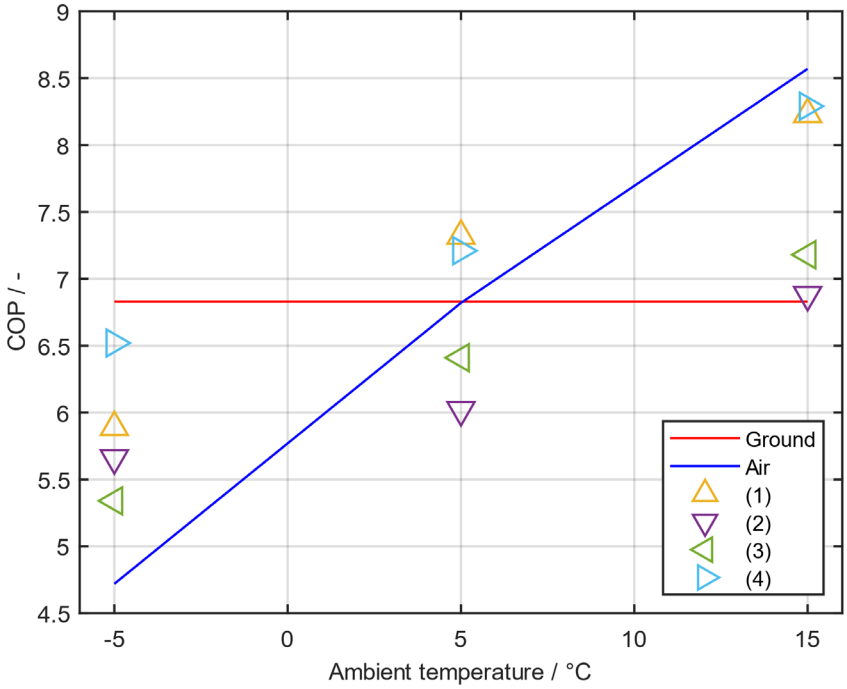

***Figure 3**: COP comparison of the different interconnections at different ambient temperatures.*

Figure 4 shows the heating power versus the ambient temperatures. A similar behavior can be observed: Interconnections (2) and (3) only show a small improvement of the heating power at low ambient temperatures and lower heating powers at similar evaporation temperatures. At high ambient temperatures, especially interconnection (2) shows almost no improvement due to the parallel operation. The reason is a high refrigerant mass flow through the GSHX and a low refrigerant mass flow through the ASHX to achieve similar overheating temperatures

through either evaporator. This is due to the overheating control of the expansion valve with the different heat source temperatures. Interconnections (1) and (4) show clear improvements at similar evaporation temperature and almost the same heating power at high ambient temperatures. Again, at low ambient temperatures, interconnection (4) shows a clear advantage, almost reaching similar heating power as the sole GSHP operation.

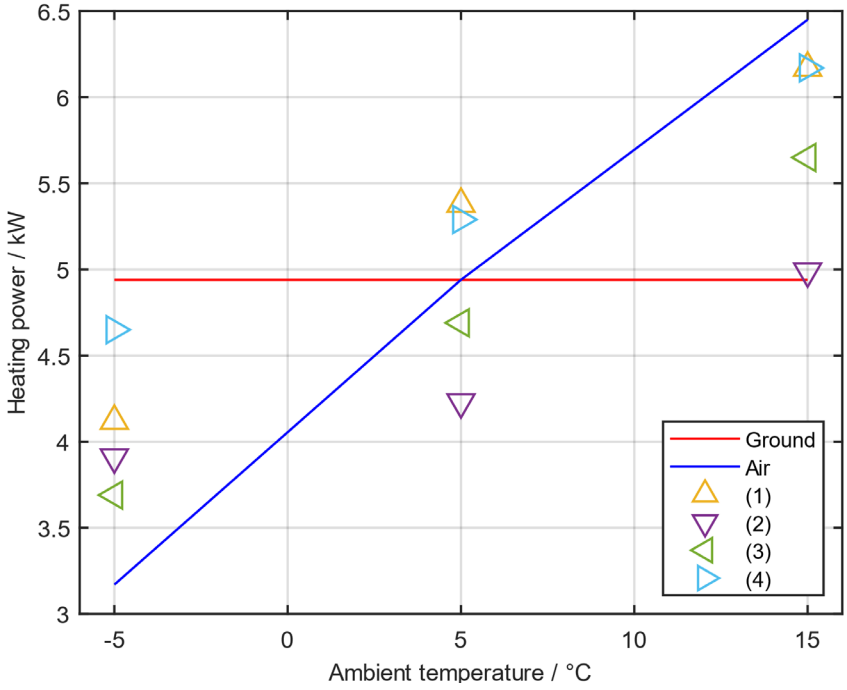

***Figure 4**: Heating power comparison of the different interconnections at different ambient temperatures.*

3.2 Heat source load comparison

The second important comparison is the loads on the heat sources. The GSHX evaporation power reduction allows a limitation of the required surface area of the GSHX, thus a smaller installation, both power- and energy-wise. An ASHX evaporation power reduction allows a limitation of ventilator speed and thus a reduction of the noise emissions.

Figure 5 shows the GSHX evaporation power required by the interconnections. First, all interconnections require less load on the GSHX independent of the ambient temperatures. At similar evaporation temperatures (with brine and ambient air inlet temperatures at 5 °C), the differences between the interconnections are minor, whith interconnection (1) showing the highest and (2) the lowest load on the GSHX. At high ambient temperatures, interconnections (1) and (2) show a very small load on the GSHX, while interconnections (3) and (4) show a reduction to GSHP operation of about 50%. Similarly, at low ambient temperatures interconnections (1) and (2) show a higher load on the GSHX compared to interconnections (3) and (4). This is due to the similar evaporation pressures: This always leads to a much higher temperature gradient to the higher-temperature heat source and thus a higher power (here: GSHX evaporation power), while the lower temperature heat source only has a low temperature gradient and thus a low power (here: ASHX evaporation power). Interconnection (3) reduces this tendency, even reversing the gradient, being able to reduce the GSHX load at low ambient temperatures. This behavior is due to the control of the brine evaporator pressure using the corresponding expansion valve as described in section 2. Interconnection (4) shows stable evaporation power over any ambient temperatures. This indicates an optimal operation of the GSHX independent of the ambient temperatures (or more general: the temperature gradient between the sources) and high flexibility in the source load.

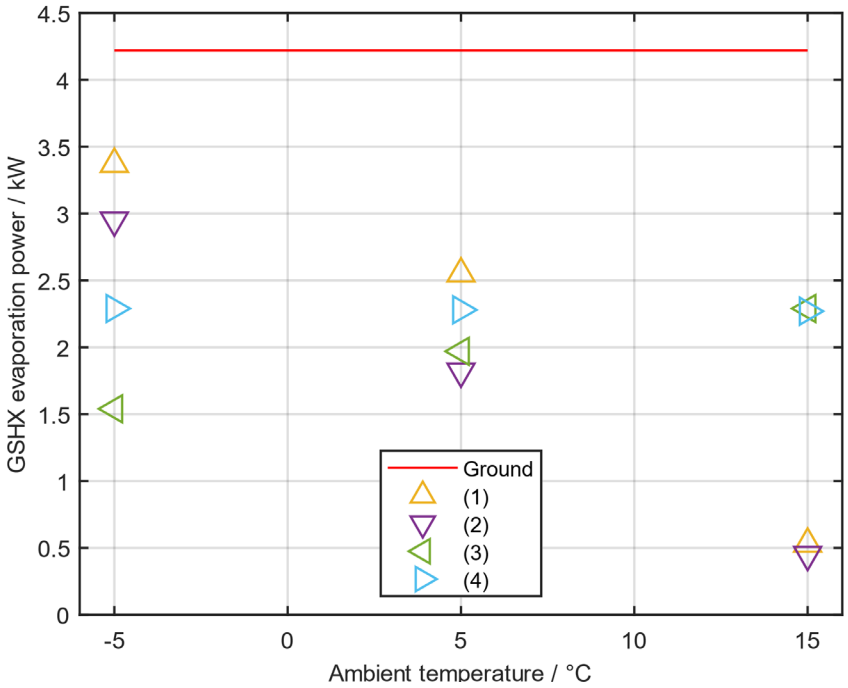

***Figure 5**: Evaporation power of the GSHX of the different interconnections at different ambient temperatures.*

This is confirmed with the evaporation load on the ASHX as shown in Figure 6. While all interconnections show a reduction of ASHX evaporation load, the interconnections (1) and (2) – interconnections on similar evaporation pressures – show almost no evaporation power of the ASHX at low ambient temperatures and higher shares of ASHX evaporation power at high ambient temperatures. Because of the similar evaporation pressures of these interconnections, there will always be a significantly higher temperature gradient to the heat source with the higher temperature. Thus, a significantly higher power is transferred, and the expansion valve control will lead to a higher refrigerant mass flow through the corresponding evaporator. Interconnections (3) and (4) show a higher share of ASHX load especially at low ambient temperatures.

4. Discussion

The selection of the optimal interconnection heavily depends on the design aims. If the aim is maximum efficiency, interconnection (1) and (4) can be used to improve the efficiency at similar ambient temperatures and at an increased temperature gradient between the heat sources (in either direction) only the single source with the higher temperature should be used. If the aim is to limit the load on the GSHX, then it depends on the temperature range where this is to be accomplished: At higher ambient temperatures, interconnections (1) and (2) have a very low GSHX evaporation load due to the similar evaporation pressures and the main evaporation load being covered by the ASHX. At low ambient temperatures interconnection (3) and (4) seem beneficial for peak heating loads. If limiting the noise emissions of the DSHP is the main requirement, the evaporation load on the ASHX should be limited: At higher ambient temperatures – contrary to the GSHX evaporation load – interconnections (3) and (4) are beneficial. At lower ambient temperatures, interconnections (1) and (2) barely use the ASHX and the ventilator could even be completely deactivated. In the series interconnections (1) and (3), the order of the sources might play a role as well, where optimization to certain boundary conditions benefits having the ASHX in front of the GSHX. This has not been further investigated yet.

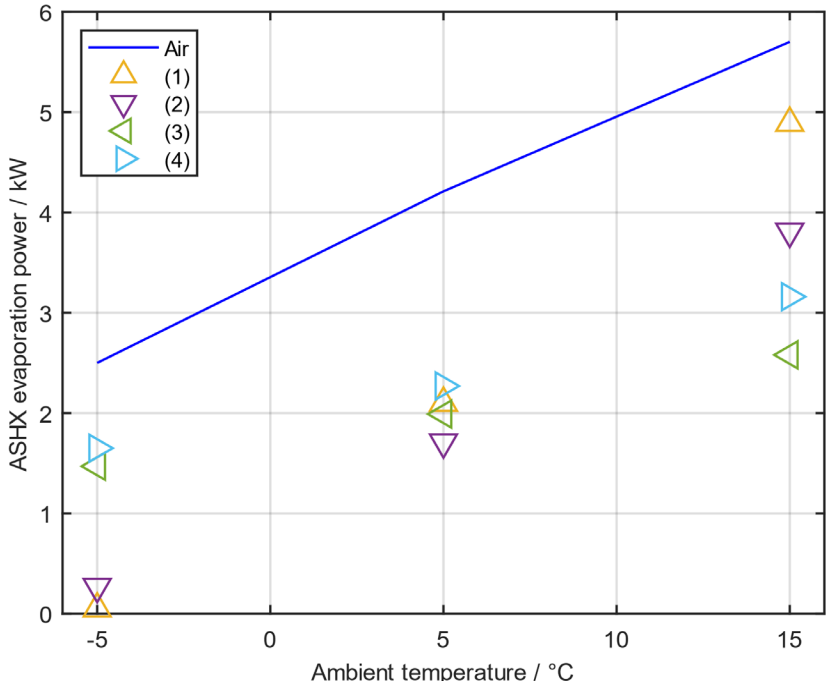

***Figure 6**: Evaporation power of the ASHX of the different interconnections at different ambient temperatures.*

For peak loads, the following requirements need to be combined: The highest possible efficiency is required, while reducing the loads on either evaporator. At low ambient temperatures, interconnection (4) clearly has the highest efficiency and heating power of the parallel operation. While ground-source operation is more efficient (about 5%) and has more heating power (about 6%), interconnection (4) is able to reduce the evaporation load on the GSHX to about 54%. At the same time, the ASHX evaporation power is reduced to about 66%, thus allowing a lower ventilator speed and therefore noise reduction.

However, for integrating a high temperature heat source (e.g. solar thermal), usually this heat source has an increased temperature compared to the other heat source and is supposed to be utilized more than the lower-temperature source. This would have a similar effect like a high ambient temperature heat source. Combining highest efficiency and maximum heating power, while also extracting the largest amount of evaporation power of the high-temperature ambient heat source (in this simulation: the ASHX, but in the case of a solar-assisted heat pump: the solar thermal collector), interconnection (1) seems most beneficial.

Interconnection (2) and (3) can have their own set of requirements, rendering them the optional solution. Especially interconnection (3) has a current limitation in the medium evaporation pressure control: The expansion valve between the evaporators is currently controlling the vapor quality. This is set to 60% vapour quality, thus yielding about 50% of the total evaporators' powers by the GSHX (assuming a vapor quality of 20% at evaporator inlet). This needs to be more closely evaluated and the control needs to be optimized. This might influence the advantages and disadvantages of this interconnection.

5. Conclusion and Outlook

The analysis of the interconnections shows significantly different energetic performances and power loads on the GSHX and ASHX depending on the boundary conditions. Temperature gradients lead to different impacts at each refrigerant cycle interconnection.

Thus, the selection of the optimal interconnection depends on the requirements of the DSHP. For the peak load coverage at high efficiency – requirement (a) – at a reduction of GSHX size

– requirement (b) – and a noise emission limitation by the ASHX – requirement (c) –, interconnection (4) seems most beneficial. Additional to the energetic arguments made in section 4., interconnection (4) also allows a highly flexible split of the evaporation power ratio: The two compressors can run at separate compressor speeds, thus directly controlling the loads on the corresponding heat source. While this setup is also assumed to require the highest investment costs (two smaller compressors including inverters are more costly than one large compressor), this can be beneficial for a high-flexibility heat source management system. For example, the load on the ASHX can be more freely controlled when an undersized GSHX is freezing during a cold period. Whether the increased investment costs for the heat pump can be recouped by lower investment costs into the GSHX and lower operational costs requires further investigation.

There are still open questions regarding this analysis: First, interconnection (3) requires a more sophisticated expansion valve control to regulate the pressure level split. Second, the simulation results need to be validated with experimental data. Third, different requirements (e.g. higher focus on noise emissions) might lead to a different final evaluation. Fourth, different heat source combinations can change the benefits due to strict temperature gradients (e.g. solar thermal collectors as a second heat source instead of either GSHX or ASHX). An annual simulation, indicating the operation modes over the year and required power by heat source, can be used as a method for this analysis. Fifth, economics need to be comprehensively investigated including investment costs into the DSHP, the GSHX and the running costs.

Data availability statement

The authors confirm that the data supporting the findings of this study are available within the article and its supplementary materials.

Author contributions

T. Reum was in charge of Conceptualization, Formal Analysis, Investigation, Visualization and Writing – original draft.

D. Schmitt contributed to Conceptualization, Formal Analysis and Writing – review & editing.

T. Summ contributed to Supervision, Project administration and Writing – review & editing.

T. Schrag contributed to Conceptualization, Supervision and Writing – review & editing.

Competing interests

The authors declare that they have no competing interests.

Funding

This work was conducted within the framework of the W^3 project, funded by the European Regional Development Fund (ERDF).

References

[1] J. Cao *et al.,* "Advances in coupled use of renewable energy sources for performance enhancement of vapour compression heat pump: A systematic review of applications to

buildings," *Applied Energy*, vol. 332, p. 120571, 2023, doi: 10.1016/j.apenergy.2022.120571.

[2] Fabian Ochs, Mara Magni and Georgios Dermentzis, F. Ochs, M. Magni, and G. Dermentzis, "Integration of Heat Pumps in Buildings and District Heating Systems—Evaluation on a Building and Energy System Level," *Energies*, vol. 15, no. 11, p. 3889, 2022, doi: 10.3390/en15113889.

[3] C. Natale, C. Naldi, M. Dongellini, and G. L. Morini, "Dynamic modelling of a dual-source heat pump system through a Simulink tool," *J. Phys.: Conf. Ser.*, vol. 2385, no. 012090, 2022, doi: 10.1088/1742-6596/2385/1/012090.

[4] K. Allaerts, M. Coomans, and R. Salenbien, "Hybrid ground-source heat pump system with active air source regeneration," *Energy Conversion and Management*, vol. 90, pp. 230–237, 2015, doi: 10.1016/j.enconman.2014.11.009.

[5] J. M. Corberán, A. Cazorla-Marín, J. Marchante-Avellaneda, and C. Montagud, "Dual source heat pump, a high efficiency and cost-effective alternative for heating, cooling and DHW production," *International Journal of Low-Carbon Technologies*, vol. 13, pp. 161–176, 2018, doi: 10.1093/ijlct/cty008.

[6] W. Behrmann, "Hybridwärmepumpe," DE 10 2010 033 142 A1.

[7] S. Karow, "Indirekt verdampfende Wärmepumpe und Verfahren zur Optimierung der Eingangstemperatur der indirekt verdampfenden Wärmepumpe," DE 10 2007 050 446 C5.

[8] G. Qiu, X. Wei, Z. Xu, and W. Cai, "A novel integrated heating system of solar energy and air source heat pumps and its optimal working condition range in cold regions," *Energy Conversion and Management*, vol. 174, pp. 922–931, 2018, doi: 10.1016/j.enconman.2018.08.072.

[9] S. Bertsch, M. Uhlmann, and A. Heldstab, "Heat Pump with Two Heat Sources on Different Temperature Levels," *International Refrigeration and Air Conditioning Conference*, 2014.

[10] T. Reum, T. Summ, M. Ehrenwirth, and T. Schrag, "Experimental Investigation of a Novel Hybrid Heat Pump," *EuroSun2022 Proceedings*, 2023, doi: 10.18086/eurosun.2022.08.11.

[11] AREA COOLING SOLUTIONS SA, *Datasheet KTN150D42UFZ.* Accessed: Oct. 6 2023. [Online]. Available: https://areacooling.com/p/ktn150d42ufz/

[12] Chemours Netherlands B.V., *Datasheet Opteon XL41 (R454B).* Accessed: Oct. 20 2023. [Online]. Available: https://www.climalife.co.uk/docs/Opteon-XL41-R454B-MSDS-v3.4.pdf